ELSEVIER

NeuroImage

www.elsevier.com/locate/ynimg
NeuroImage 32 (2006) 570 – 582

Technical Note

Testing anatomically specified hypotheses in functional imaging using cytoarchitectonic maps

Simon B. Eickhoff,[a,b,*] Stefan Heim,[a,c] Karl Zilles,[a,b,c] and Katrin Amunts[a,c,d]

[a] *Institut für Medizin, Forschungszentrum Jülich, Jülich, Germany*
[b] *C. and O. Vogt Institut für Hirnforschung, Düsseldorf, Germany*
[c] *Brain Imaging Center West (BICW), Jülich, Germany*
[d] *Klinik für Psychiatrie und Psychotherapie, RWTH Aachen University, Germany*

Received 22 November 2005; revised 27 February 2006; accepted 5 April 2006
Available online 14 June 2006

The statistical inference on functional imaging data is severely complicated by the embedded multiple testing problem. Defining a region of interest (ROI) where the activation is hypothesized *a priori* helps to circumvent this problem, since in this case the inference is restricted to fewer simultaneous tests, rendering it more sensitive. Cytoarchitectonic maps obtained from postmortem brains provide objective, *a priori* ROIs that can be used to test anatomically specified hypotheses about the localization of functional activations. We here analyzed three methods for the definition of ROIs based on probabilistic cytoarchitectonic maps. (1) ROIs defined by the volume assigned to a cytoarchitectonic area in the summary map of all areas (maximum probability map, MPM), (2) ROIs based on thresholding the individual probabilistic maps and (3) spherical ROIs build around the cytoarchitectonic center of gravity. The quality with which the thus defined ROIs represented the respective cytoarchitectonic areas as well as their sensitivity for detecting functional activations was subsequently statistically evaluated. Our data showed that the MPM method yields ROIs, which reflect most adequately the underlying anatomical hypotheses. These maps also show a high degree of sensitivity in the statistical analysis. We thus propose the use of MPMs for the definition of ROIs. In combination with thresholding based on the Gaussian random field theory, these ROIs can then be applied to test anatomically specified hypotheses in functional neuroimaging studies.

Keywords: fMRI; Structure; Mapping; Gaussian random fields; ROI

Introduction

Functional neuroimaging such as positron emission tomography (PET) or functional magnetic resonance imaging (fMRI) is based on changes in cerebral blood flow or metabolism measured in subjects scanned repeatedly under different experimental conditions. In order to identify brain regions which show significant signal differences between those conditions, a univariate model is fitted independently to each voxel of the volume. Voxels where the subsequently computed test statistic exceeds an defined threshold are then classified as active in this particular contrast. This approach, however, embodies a massive multiple testing problem as up to 100,000 test statistics (corresponding to the analyzed voxels) have to be assessed simultaneously. Using an α-level of 0.05 for these tests implicates a 5% chance of falsely rejecting the null hypothesis. Thus, up to 100,000 * 0.05 = 5000 voxels would be declared active, even if there were no signal in the data. The situation is further complicated by the fact that the individual test statistics are highly correlated. Accordingly, Bonferroni's correction for multiple comparisons would be overly conservative since it would overestimate the true number of independent observations.

This problem has been solved by the introduction of Gaussian random field theory (GRF) into neuroimaging. As described in the seminal paper by Worsley et al. (1996), statistical parametric maps can be interpreted as lattice representation of an underlying random field. Thresholds corrected for the family wise error rate (FWE), i.e., the average chance of *any* false positive activation, can then be derived from these fields. These thresholds are based on Euler's characteristics of the excursion set, e.g., the expected number of "peaks" in the thresholded random field. The necessary threshold to correct for a specified FWE rate depends on the type and smoothness of the random field and on the assessed region of interest (ROI). Evidently, smaller ROIs comprise fewer multiple tests and require a lower threshold. Thus, if the search volume can be confined to a specific brain region where activation is hypothesized, the sensitivity of the analysis increases. This procedure, known as small volume correction (SVC), can be used to reveal more subtle activations. Since the ROIs for small volume correction have to be specified *a priori*, they are commonly defined as spheres of user-specified radius around the coordinates of previously reported activations for similar tasks. Often, however, the expected locali-

* Corresponding author. Institut für Medizin, Forschungszentrum Jülich GmbH, D-52425 Jülich, Germany. Fax: +49 2461 61 2820.
E-mail address: S.Eickhoff@fz-juelich.de (S.B. Eickhoff).
Available online on ScienceDirect (www.sciencedirect.com).

1053-8119/$ - see front matter © 2006 Elsevier Inc. All rights reserved.
doi:10.1016/j.neuroimage.2006.04.204

zation of activation also is framed as an *anatomical* hypothesis, e.g., "We expect area 44 to be activated". However, testing for activation in, e.g., area 44 using a spherical ROI is not an optimal solution, because this ROI will include neighboring cortical areas and white matter as well. Thus, a significant portion of the activation obtained through small volume correction for "area 44" might actually be located in, e.g., area 6.

Incorporating data from anatomical brain mapping studies may circumvent these problems and yield anatomically more valid ROIs. This idea has motivated the generation of ROIs based on the Talairach and Tournoux atlas (Lancaster et al., 2000; Maldjian et al., 2003; Talairach and Tournoux, 1988). However, the obtained results are limited by the major drawbacks of the Talairach atlas, e.g., the tentative transfer of Brodmann's drawing (Brodmann, 1909) to a dissected and photographed postmortem reference brain, the different reference system used by this atlas as compared to functional neuroimaging or the missing information about the inter-individual variability in size and location of cortical areas (Eickhoff et al., 2005). In contrast to the Talairach atlas, probabilistic cytoarchitectonic maps (Amunts and Zilles, 2001; Amunts et al., 2004; Eickhoff et al., 2005; Zilles et al., 2002, 2003; Fig. 1) provide stereotaxic information on the location and variability of cortical areas. They are based on an observer-independent cytoarchitectonic analysis in a sample of 10 human postmortem brains which were subsequently spatially normalised to the anatomical MNI reference space. This space differs from the original MNI reference space (Collins et al., 1994; Evans et al., 1992; Holmes et al., 1998), which is a widely used reference system in functional neuroimaging, by an affine translation along the y and z axes of 4 and 5 mm, respectively. This shift was introduced in

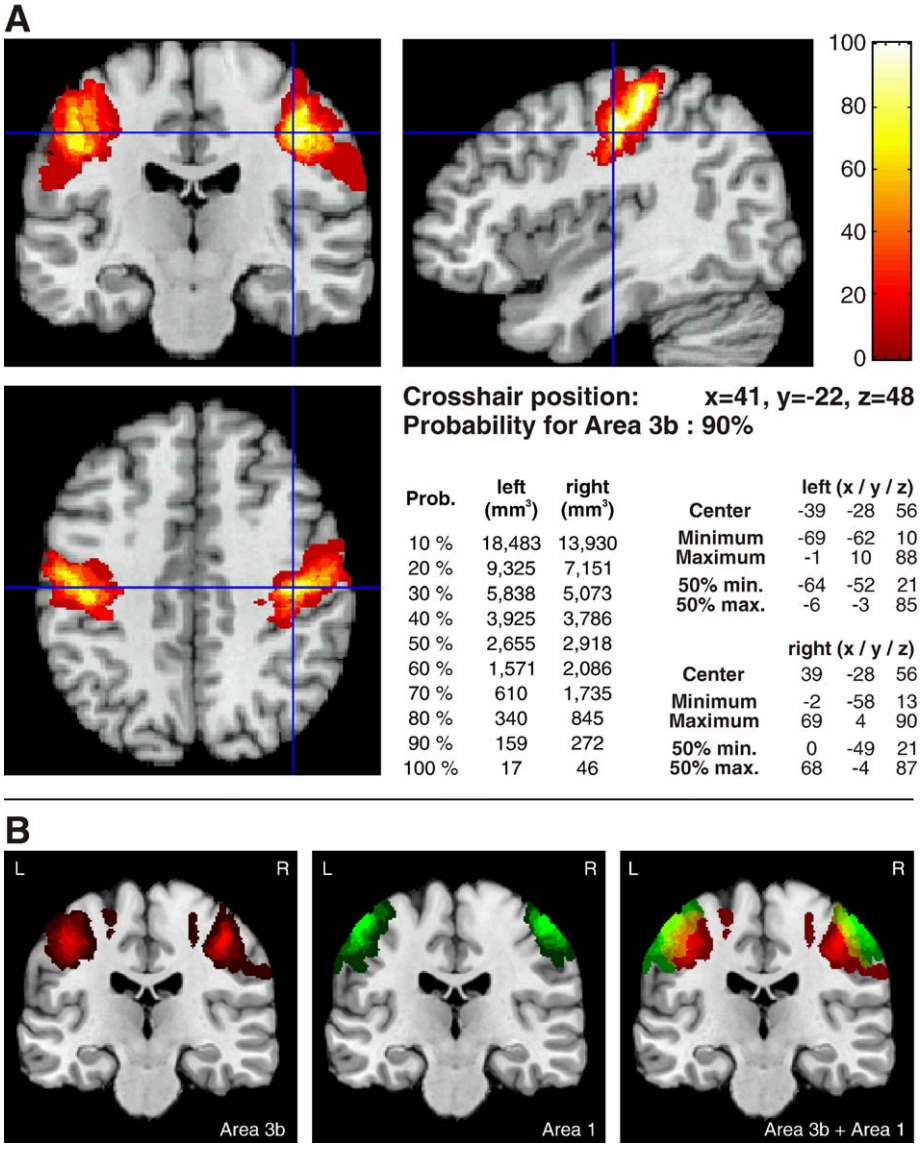

Fig. 1. (A) Orthogonal sections and statistics for the probabilistic map of area 3b (Geyer et al., 2000) as provided by the SPM Anatomy toolbox (Eickhoff et al., 2005). All coordinates are in anatomical MNI space (i.e., origin defined by the AC, cf. Eickhoff et al., 2005). (B) Coronal sections through the T1-weighted MNI single-subject template at $y = -25$ in anatomical MNI space (i.e., $y = -21$ in the original MNI space), showing the probabilistic maps of area 3b (left) and area 1 (middle). Note the considerable overlap in the probabilistic maps of these two (neighboring) cortical areas illustrated in right panel, which shows both probabilistic maps superimposed on each other.

order to relocate the origin of the coordinate system to the anterior commissure of the T1-weighted MNI single subject template (Eickhoff et al., 2005). The advantage of the anatomical MNI space is the correspondence of its origin with that of the atlas system of Talairach and Tournoux (1988), where the x, y and z coordinates indicate the distance in millimeters from the anterior commissure, a clearly defined anatomical landmark. The MNI space and the anatomical MNI space do not differ with respect to any other linear or non-linear transformation. The anatomical MNI space is thus preferable to the "Talairach space" (Talairach and Tournoux, 1988), which shows significant differences to the MNI space not only in the size but also in the shape of the reference brain, rendering a coordinate-based comparison between them difficult or even impossible (Brett et al., 2002; Chau and McIntosh, 2005).

Anatomical ROIs based on probabilistic cytoarchitectonic maps can therefore provide *a priori* information for the assessment of anatomically specified hypotheses by functional imaging studies. This has been shown in the last few years by a rapidly growing number of studies successfully using probabilistic cytoarchitectonic maps in combination with fMRI and PET data (e.g., Amunts et al., 2004; Bodegard et al., 2000; Eickhoff et al., in press; Grol et al., 2006; Heim et al., 2005; Horwitz et al., 2003; Hurlemann et al., 2005; Kell et al., 2005; Naito et al., 1999, 2005; Noppeney et al., 2005; Young et al., 2004, Larsson et al., 1999; Binkofski et al., 2000). It seems to be intuitive that ROIs based on cytoarchitectonic probabilistic maps of cortical areas are superior to spherical ROIs or macroanatomical landmarks such as gyri and sulci, in the representation of areal specific hypothesis. However, the influence of different methods for the definition of ROIs has not yet been evaluated. Therefore, the aim of this paper was the comparison and evaluation of different procedures for the definition of binary ROIs from probabilistic cytoarchitectonic maps. Procedures were evaluated both with respect to the quality with which the defined ROIs reflect the underlying anatomical hypothesis, and with respect to their sensitivity for detecting functional activations.

Materials and methods

A maximum probability map (MPM, Eickhoff et al., 2005) is a summary map of different probabilistic cytoarchitectonic maps. It is based on the idea of attributing each voxel of the reference space to the most likely cytoarchitectonic area at this position (Fig. 2). MPMs thus allow the definition of non-overlapping representations of all areas from a set of inevitably overlapping probabilistic maps (cf. Fig. 1B). ROIs can be defined from the MPM by a simple binarization: All voxels which are assigned to those areas that should be included in the ROI are set to "1" and the rest the value "0" (Fig. 3).

Anatomical ROIs can also be defined by thresholding an individual probabilistic map. For example, an ROI representing area 3b can be defined by those voxels, where area 3b is found with a probability (i.e., relative frequency) of $\geq$50% (Figs. 1 and 3). Finding an appropriate threshold is by itself an ambiguous task as the volume associated with a cortical area increases substantially at lower thresholds (Fig. 1, Table 1). Lower thresholds therefore overestimate the areal volume and have a relatively low anatomical specificity. For example, the mean probability for area 3b within an ROI defined by thresholding its probabilistic map at 20% probability is only 39%, while the size of that ROI is more than twice the mean size of area 3b (Table 1). Higher thresholds on the other hand show a high anatomical specificity but underestimate the size of the respective area. For example, the 80% map of area 3b represents only a tenth of its mean volume. Consequently, only intermediate thresholds of 40 or 50% can be considered suitable for defining anatomical ROIs (Fig. 3).

In analogy to the conventional approach for small volume corrections, ROIs can also be defined by spheres. The localization of these spheres can in turn be determined by the center of gravity of the probabilistic maps (Fig. 3).

Comparison of the methods

The defined ROIs were compared with respect to their quality of anatomical representation (measures I–IV below) and their sensitivity to detect functional activations (measure V).

Mean probability within the ROI

The mean probability for finding the hypothesized area within the ROI should be as high as possible. The rationale behind this measure is that a higher mean probability within an ROI will increase the likelihood that an observed significant activation within this ROI does indeed originate from the hypothesized area.

Deviation of the ROI volume from mean volume

This measure is defined as the size of the ROI relative to the mean volume of the respective area after spatial normalization (in MNI space), expressed in percent. A value of less than 100% indicates that the ROI is smaller than the average size of that area,

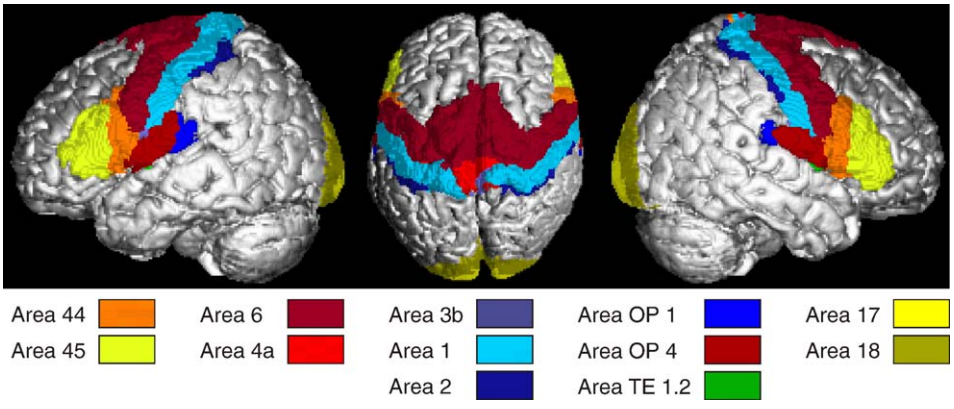

Fig. 2. Surface rendering of the T1-weighted MNI single-subject template and the MPM (MPM) of all probabilistic maps of cortical areas published to date. Only the surface extent of the different areas is shown. (a) Lateral view on the left hemisphere, (b) dorsal view, (c) lateral view on the right hemisphere.

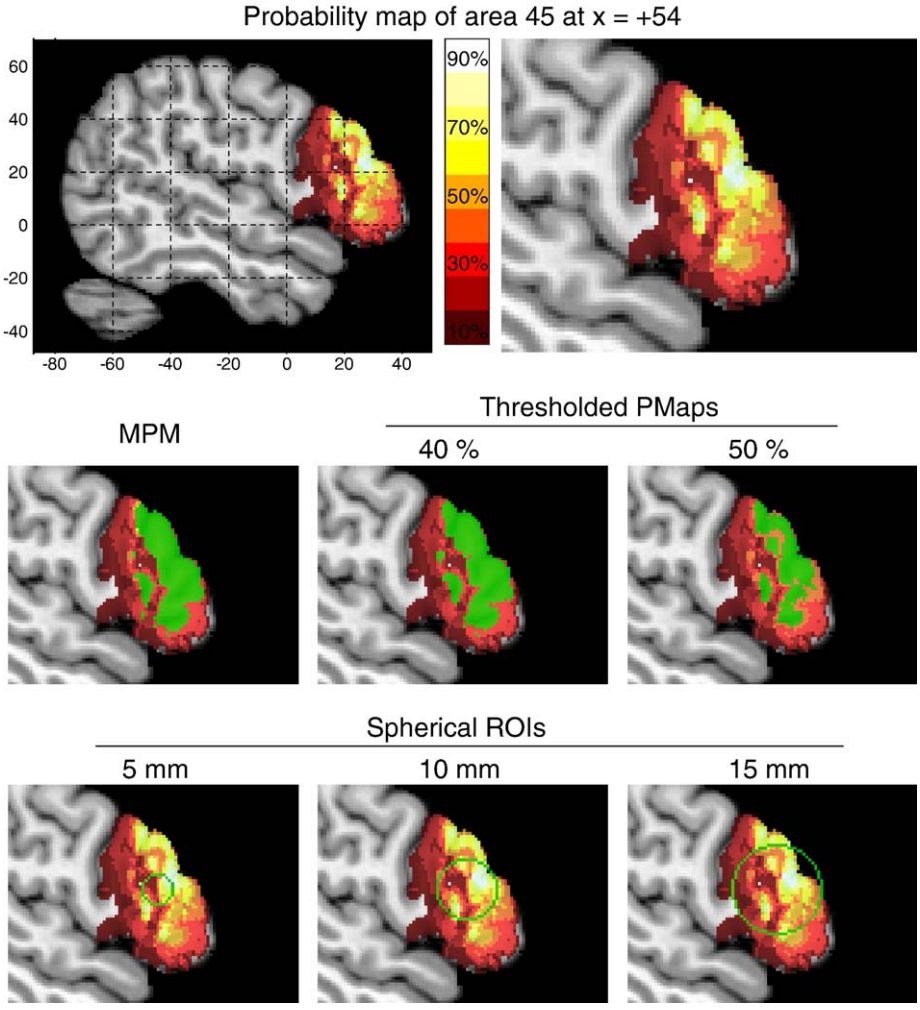

Fig. 3. Visualization of the different methods for defining ROIs (shown in green in the middle and lower row) for an anatomically defined cytoarchitectonic area from its probabilistic map. Upper row: Saggital section through the probabilistic map of Broca's area 45 on the right hemisphere at $x = +45$ shown on the coordinate grid of the anatomical MNI space (Eickhoff et al., 2005); color bar indicating the probability levels of coded by the different colors; and a detail view of that section displaying the same region as shown in the two lower rows. Middle row: The green color marks those voxels that are included in the ROI representing area 45 based on the MPM (MPM, left), by thresholding at 40% probability (middle) and 50% probability (right). Lower row: The green circles indicate the extend of a spherical ROI of the shown radius around the center of gravity of area 45. Voxels inside the circles are included in the resulting ROIs.

values of more than 100% denote ROIs that are larger than the mean volume. Ideally, an ROI would be of the same size as the area itself (i.e., 100% of the mean volume in MNI space).

Fraction of misclassified voxels

As illustrated in Fig. 1B, there is a substantial overlap between the probability maps of different cortical areas. Thus, several voxels in a defined ROI might be associated with more than one cortical area. Naturally, an ROI constructed to represent an areal specific hypothesis should include as few voxels as possible from neighboring cortical areas. Accordingly, the fraction of misclassified voxels (defined as the percentage of voxels in the ROI where a different area was observed more likely than the hypothesized one) is also used for measuring the quality of anatomical representation.

Overall areal coverage

The 'overall areal coverage' indicates the relative amount of all cytoarchitectonic observations for a given area that are represented by the ROI. It thus represents a summary measure indicating how well an ROI covered the respective cytoarchitectonic area. The 'overall areal coverage' is calculated by multiplying the number of voxels in the ROI where the hypothesized cytoarchitectonic area was indeed found most likely (i.e., excluding misclassified voxels) by the mean probability for the respective area within these voxels. This yields the volume of the respective area, which is correctly represented by the ROI. This value is then normalizing by the mean histological volume of that area. The 'overall areal coverage' therefore represents a synopsis of the measures I–III defined above: to reach high values in the 'overall areal coverage', an ROI should not be overly restrictive, contain as few misclassified voxels as possible and have a high mean probability for the examined area.

Sensitivity of the defined ROIs

The sensitivity to functional activations was parameterized by the lowest t value declared significant when correcting for multiple comparisons in the ROI volume (critical value). The

Table 1
Comparison of the ROIs defined by thresholding the probabilistic map of right primary somatosensory area 3b (Geyer et al., 2000) at different probability levels

Threshold	Size		Mean probability
	mm³	% of mean	
10%	37,842	352	28
20%	23,912	223	39
30%	16,761	156	47
40%	11,688	109	54
50%	7902	73	61
60%	4984	46	68
70%	2898	26	75
80%	1163	10	83
90%	318	2	91
100%	46	<1	100

A threshold of 40% is equivalent to including only those voxels, where area 3b was found in at least 4 out of the 10 histologically examined brains. The resulting regions are characterized in terms of their absolute size (in mm³), their size relative to the mean volume after non-linear normalization (shown in percent) and by the mean probability for finding area 3b in these ROI.

rationale behind this approach is that the critical value depends only on the examined ROI (assuming the same smoothness, statistical field, multiple comparison method and significance level). It can therefore be regarded as a direct measure of its sensitivity. The smoothness of functional imaging data can be approximated by the harmonic mean between its intrinsic smoothness (approximately the voxel size at image acquisition, i.e., 3–5 mm) and the full width at half maximum (FWHM) of the explicitly applied spatial smoothing kernel (8–12 mm). Typical smoothness values for fMRI data thus range from 8.5 to 13 mm. In our analysis, we first focussed on an intermediate level of smoothness (FWHM = 11 mm). Subsequently, smoothness values of 8.5 and 13 mm FWHM were assumed to analyze the possible dependence of the obtained results on the smoothness of the data. All critical values were calculated for a T-distribution with 15 degrees of freedom, simulating a second level mixed effects analysis using a one-sample t test on images from 16 subjects, which are common figures in fMRI (Penny and Holmes, 2003). In our simulated analysis, the critical value (i.e., the lowest t value passing a multiple comparison correction in the ROI) was computed for a family wise error rate corrected threshold of $P < 0.05$ (Worsley et al., 1996; Worsley, 2003).

Exemplary analysis of three cortical areas

Analysis of differences between the various ROIs is hampered by the fact that cortical areas differ between each other with respect to their size and geometry. For example premotor area 6, the largest area mapped up to date (Geyer, 2003), is on average more than 40 times as large as auditory area TE 1.2 (Morosan et al., 2001). Some larger cortical areas (e.g., areas 44 and 45) have an extended cortical surface and thus (due to the convexity of the brain) a shell-shaped, hull-like structure. Other areas, in particular those located on the pre- and postcentral gyrus (areas 4a, 4p, 3a, 3b, 1, 2), have a thin but elongated configuration. This stripe-like configuration causes large surface areas relative to the areal volumes. Finally, some areas, like OP 2 and OP 3 on the parietal operculum (Eickhoff et al., 2006a,b), or primary auditory areas TE 1.1 and TE 1.2 (Morosan et al., 2001) are smaller and more compact (i.e., the size of these areas in the different spatial directions is similar).

In order to evaluate the influence of these differences on the ROI definition, the ROIs for three cortical areas (all on the right hemisphere) representing different areal geometries will be presented in detail: Area 45 (Amunts et al., 1999; Fig. 4A) was chosen to represent large cytoarchitectonic areas, with an extended cortical surface. Primary somatosensory area 3b (Geyer et al., 2000; Fig. 4B) on the other hand is a medium sized area, which has an elongated, stripe like structure. Area TE 1.1 of the primary auditory cortex (Morosan et al., 2001; Fig. 4C) was chosen as an example of a small compact area.

Statistical analysis of the differences between the defined ROIs

Subsequently, we tested statistically which of the measures defined were significantly affected by the choice of the ROI definition. Eighteen cortical areas were examined: somatosensory areas 3a, 3b, 1 and 2 (Geyer et al., 1999, 2000; Grefkes et al., 2001); precentral areas 4a, 4p and 6 (Geyer et al., 1996; Geyer, 2003); areas 44 and 45 (Amunts et al., 1999); parietal opercular areas OP 1, OP 2, OP 3 and OP 4 (Eickhoff et al., 2006a,b); TE 1.0, TE 1.1 and TE 1.2 of the primary auditory cortex (Morosan et al., 2001; Rademacher et al., 2001) and visual areas 17 and 18 (Amunts et al., 2000). Since a separate ROI was computed for each hemisphere, 36 individual ROIs were assessed. Each of these ROIs was constructed by the three methods based on probabilistic cytoarchitectonic maps (MPM, 40% and 50% maps). In order to test whether a one of the five measures (I–V, cf. above) was significantly different between the three types of ROIs (representing the same anatomical area), a one-way repeated measurement ANOVA was applied. If there was a significant overall effect of the factor “ROI definition method”, we used a subsequent pairwise multiple comparison procedure to identify those methods that were significantly different from each other ($P < 0.05$, corrected for multiple comparisons). The test statistic of the post-ANOVA Tuckey test (q) is found by dividing the difference between the means $\bar{x}_i - \bar{x}_j$ by the square root of the ratio of the within group variation (S_w^2) and the sample size (n) (Timm, 2002).

$$q = \frac{\bar{x}_i - \bar{x}_j}{\sqrt{s_w^2/n}}$$

Empirical fMRI data example

The applicability of the proposed cytoarchitectonic ROIs in combination with functional imaging data, and the advantages of the proposed approach – as compared to spherical ROIs – are demonstrated using an fMRI experiment of tactile stimulation of 3 subjects. The block-design consisted of 11 cycles of approximately 18 s stimulation (brushing the subject’s left hand at ~2 Hertz with a sponge) followed by 18 s of resting state baseline, during which no stimulation was applied. EPI images were acquired on a Siemens Vision 1.5 T scanner (Erlangen, Germany) using blood-oxygen-level-dependent (BOLD) contrast [Gradient-echo EPI pulse sequence, TR 3 s, resolution: 3.1 × 3.1 × 3.1 mm³, 30 axial slices]. High-resolution (1 mm³ voxel) T1-weighted 3D MP-RAGE images were also acquired, and coregistered to the EPI images. Preprocessing (realignment, coregistration, normalization into MNI space, 8 mm FWHM Gaussian smoothing) and statistical analysis by

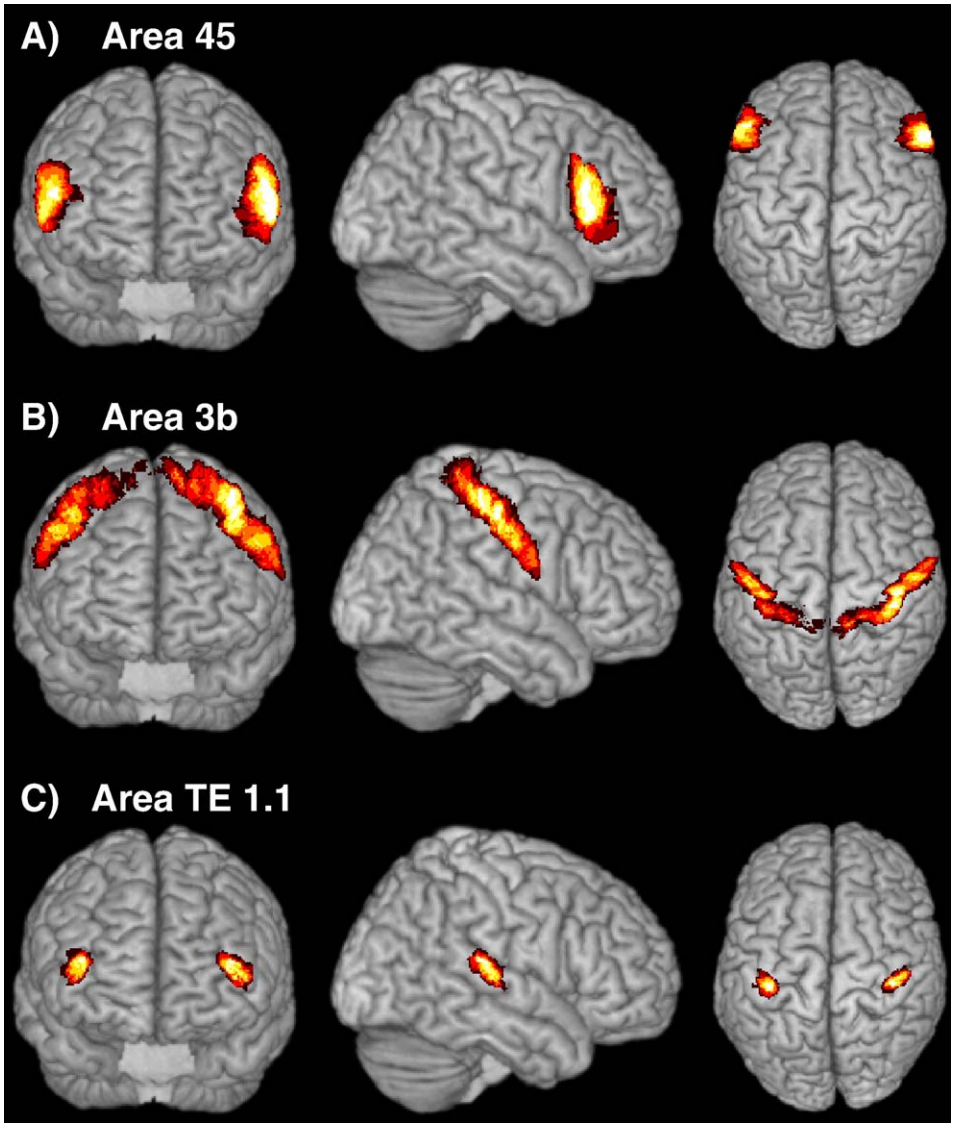

Fig. 4. Maximum intensity projections of the cytoarchitectonic probability maps of area 45 (A), primary somatosensory are 3b (B) and TE 1.1 of the primary auditory cortex (C) onto a surface rendering of the MNI single subject template brain, which illustrate the different geometries of the three areas. Only voxels that had a probability of at least 40% are shown for the sake of clarity.

means of a general linear model using a boxcar model convolved with a canonical hemodynamic response function (Kiebel and Holmes, 2003) were performed using SPM5 (http://www.fil.ion.ucl.ac.uk/spm). After evaluating of the contrast "tactile stimulation vs. a resting state baseline", inference on the respective SPM{T} map was performed three time: (1) Using a brain wide family wise error rate correction of $P < 0.05$. (2) Using a small volume correction for right Area 3b, as defined by the representation of this area in the Maximum Probability Map (MPM). (3) Using a spherical ROI, centered on the mean coordinates for Area 3b on the right hemisphere. At the beginning, we use a sphere with a radius of 15 mm as an ROI, since the volume of this sphere is closest to the mean histological volume of this area as shown in (Table 2). Since no cortical activation was observed within a spherical search volume of 15 mm radius around the mean coordinates (due to the curvature of the cerebral hemispheres, the sphere was basically hidden in the white matter), the analysis was subsequently repeated using a 20 mm sphere.

Results

Exemplary analysis of three cortical areas

The mean probabilities for areas 3b, TE 1.1 and 45 within the anatomically defined ROIs (MPM, 40% map, 50% map) ranged from 52% to 69%. For all three areas, the mean probabilities within the MPM were similar to those within the 40% maps (Table 2). The mean probabilities in the 50% maps, however, were 4 to 9% higher than those within the MPM or the 40% maps. The mean probabilities within the 5 mm spheres (56%, 53% and 65% respectively) were within the range of the values obtained for anatomically defined ROIs (MPM, 40% map, 50% map). The mean probabilities within the larger spheres were, in particular for area TE 1.1, considerably lower (Table 2).

The volumes of the MPM-based ROIs were always smaller than the volumes of the 40% maps but larger than those of the 50% maps. The volumes of 40% maps and MPM-based ROIs did not

Table 2
Comparison of the different ROI definitions for three exemplary cortical areas: area 45 (Amunts et al., 1999), area 3b (Geyer et al., 2000) and area TE 1.1 (Morosan et al., 2001)

	Size		Anat. specificity			t ($P < 0.05$)
	mm^3	% of mean	Mean probability (%)	Misclassified (%)	'Overall areal coverage' (%)	
Area 45 (mean volume 6959 mm^3)						
MPM	6596	97	58	<0.1	57	4.64
40%	6874	101	58	7	55	4.69
50%	4922	71	65	3	44	4.52
5 mm	525	7	56	0.3	2	3.11
10 mm	4196	61	46	4.5	24	4.12
15 mm	14,152	207	28	13.5	50	4.84
Area 3b (mean volume 11,137 mm^3)						
MPM	9710	91	52	0.8	47	4.96
40%	11,688	109	54	31	40	5.06
50%	7902	73	61	19	35	4.87
5 mm	525	4	53	49	1	3.11
10 mm	4203	39	34	68	3	4.12
15 mm	14,162	132	21	77	5	4.84
Area TE 1.1 (mean volume 1873 mm^3)						
MPM	1808	98	65	<0.1	63	3.92
40%	2079	112	62	14	59	3.98
50%	1606	86	69	6	55	3.86
5 mm	520	27	65	0.9	15	3.11
10 mm	4181	225	31	35	44	4.12
15 mm	14,105	759	12	44	50	4.84

The ROIs are characterized in terms of their absolute (mm^3) and relative (percent of the mean volume) size, the mean probability for the respective area in the ROI, the percentage of misclassified voxels (i.e., voxels, where another area was found more likely) and the summary measure indicating the relative amount of all cytoarchitectonic observations (in any postmortem brain) for this area captured by the ROI excluding misclassified voxels. The last column shows the lowest t value that will be declared significant when correcting for multiple comparisons in the defined ROI indicating the sensitivity to functional activations.

deviate more than 12% from the mean volume of the respective areas (Table 2). The 50% maps represented area TE 1.1 reasonably well (covering 86% of the mean volume) but underestimated the sizes of areas 45 and 3b by more than a forth. Spheres with a radius of 5 or 10 mm only included a small proportion of the mean volumes of areas 45 and 3b. Larger spheres (15 mm radius) considerably overestimated the volume of all three areas (Table 2). The volume of area TE 1.1 was overestimated more than twofold by both the 10 and 15 mm spheres. The spherical ROI with a radius of 5 mm, on the other hand, covered only 27% of the mean volume of area TE 1.1.

The MPM-based ROIs virtually contained no misclassified voxels (Table 2). The small amount of misclassified voxels present in the MPMs (e.g., 0.8% for area 3b) is due to the fact that the computed MPM is low pass filtered in order to yield spatially continuous representations. That is, voxels that are surrounded by other voxels which are assigned a different area are reassigned to the latter area. ROIs based on 50% maps and in particular those based on 40% maps, however, contained between 3% (50% map of area 45) and 31% (40% map of area 3b) misclassified voxels. The fraction of misclassified voxels in the smaller spheres representing area 45 was lower than that in the 40% map (Table 2). The fraction of misclassified voxels in the 5 mm sphere representing area TE 1.1 was only 0.9%. Larger spheres, however, contained a high amount of misclassified voxels (Table 2). For area 3b, the fraction of misclassified voxels in the spherical ROIs was considerably higher.

The 'overall areal coverage' provided by the MPM was always the highest among the anatomically defined ROIs. The 40% maps ranked next, while the 50% provided the lowest coverage of all three areas. For areas 45 and TE 1.1, the largest spheres also provided a relatively good coverage. However, their 'overall areal coverage' was always lower than that provided by the MPM-based ROIs. The 'overall coverage' of area 3b by spherical ROIs, on the other hand, was maximally 5%.

For area 45, the minimum t statistic declared positive after multiple comparisons correction within the MPM-based ROI was 4.64 (Table 2). The sensitivity of the 50% map was slightly higher (critical threshold 4.52), while that of the 40% map was slightly lower (critical threshold 4.69). These results were confirmed by the analysis of the ROIs representing areas 3b and TE 1.1. The 50% maps always required lowest corrected thresholds and can thus be considered to be most sensitive. The MPM-based ROIs in turn consistently required less conservative thresholds than the 40% maps. The corrected thresholds for the spherical ROIs were in general lower than those required for anatomically defined ROIs. For example, the lowest threshold for an anatomically defined ROI representing area 3b was 4.87. A sphere of 15 mm radius, however, which was 20% larger in volume than even the largest of the defined ROIs only required a threshold of 4.84. A similar observation was made for area TE 1.1. A spherical ROI with a radius of 10 mm was more than twice as large as the ROI defined by the 40% map but required only a slightly higher corrected threshold (4.12 vs. 3.98).

Statistical analysis of the differences between the defined ROIs

The evaluation of areas 45, 3b and TE 1.1 showed that spherical ROIs represent anatomical hypotheses less adequately than MPM-

based ROIs and thresholded probabilistic maps. They were thus not included in the subsequent statistical analysis, in which the five measures defined above were computed for 36 ROIs (18 areas, both hemispheres). A graphical representation of the effects of the ROI definition method (MPM, 40% and 50% maps) on the quality of anatomical representation and the functional sensitivity is given in Fig. 5. The statistical analysis revealed a significant effect of the factor "ROI defining method" on each of the five analyzed measures (F test, $P < 0.001$).

I) The relative volume deviation (Fig. 5A) was significantly smaller for ROIs defined by the MPM or 40% maps than for ROIs defined by 50% maps ($q = 6.34$ for MPM vs. 50%; $q = 8.29$ for 40% vs. 50%, $P < 0.05$; all P values corrected for multiple comparisons). The volume deviation of the 40% maps was not significantly different from that of the MPM-based ROIs ($q = 1.95$, $P > 0.05$).

II) The mean probabilities (Fig. 5B) were not significantly different between the 40% maps and the MPM ($q = 1.67$, $P > 0.05$). The mean probabilities in the 50% map ROIs, on the other hand, were significantly higher than those found in 40% maps or MPM-based ROIs ($q = 21.73$ for 50% vs. MPM and $q = 23.40$ for 50% vs. 40%, $P < 0.05$).

III) The analysis of the fraction of misclassified voxels (Fig. 5C) revealed that the MPM-based ROIs contained significantly less misclassified voxels than both 40% or 50% maps ($q = 25.14$ for MPM vs. 40% and $q = 14.56$ for MPM vs. 50%, $P < 0.05$). The 50% maps in turn contained significantly less misclassified voxels than the 40% maps ($q = 10.58$, $P < 0.05$).

IV) The 'overall areal coverage' (Fig. 5D) of the MPM-based ROIs was significantly greater compared to that of the 40% maps ($q = 15.69$, $P < 0.05$). Both of these methods, however, covered a significantly larger proportion of all cytoarchitectonic observations than the 50% maps ($q = 23.12$ for MPM vs. 50%, $q = 7.42$ for 40% vs. 50%, $P < 0.05$). Since the 'overall areal coverage' represents a summary of the other three measures for the quality of anatomical representation, the resulting rank order of the three ROI definition methods seen in this analysis is of particular relevance for the final decision of the most appropriate method for defining anatomical ROIs.

V) The thresholds necessary for multiple comparison correction within the ROIs (Fig. 5E) were significantly different between all methods. The 50% maps were the most sensitive, i.e., required to lowest thresholds ($q = 8.45$ for 50% vs. MPM and $q = 15.67$ for 50% vs. 40%, $P < 0.05$). However, the differences in corrected thresholds between MPM-based ROIs and 40% maps were also significant ($q = 7.21$, $P < 0.05$). Thus, the ROIs defined by the MPM representation of the respective areas were significantly more sensitive than those defined by the 40% maps.

The subsequent repetition of this sensitivity analysis with other smoothness parameters (8.5 mm and 13 mm) confirmed the obtained results (Fig. 5F). Although the absolute thresholds decrease with increasing data smoothness, the effects of the different ROI definitions remain stable. For all levels of smoothness, the 50% maps required the lowest corrected threshold, while MPMs were significantly more sensitive than 40% maps ($P < 0.05$ corrected).

fMRI data example

The fMRI results for the contrast "tactile stimulation of the left hand vs. resting state baseline" are summarized in Fig. 6. It shows that the regions that were significantly activated after correcting for the family wise error rate ($P < 0.05$) depended markedly on the search volume.

When the search volume comprised the entire brain, none of the three subjects showed a significant activation on the postcentral gyrus (Fig. 6, first column in each row). The only activation which survived the whole brain correction in two of the subjects (subjects 1 and 3) was a small activation on the parietal operculum, corresponding to the secondary somatosensory cortex.

Since an activation of the contralateral primary somatosensory cortex (i.e., right area 3b) was hypothesized *a priori*, a small volume correction was performed. The search volume was hereby confined to the MPM representation of right area 3b (cf. Table 2). The analysis revealed a distinct activation of the postcentral gyrus for all three subjects (Fig. 6, second column in each row). The location of these activations in the vicinity of the omega-shaped "hand knob" corresponds to the well established location of the hand representation in the primary somatosensory cortex (e.g., Young et al., 2004). As expected, area 3b was the most likely cytoarchitectonic area at each and every significantly activated voxel in all three subjects (the mean probability for area 3b in the activated voxels was 64%, the probabilities for areas 1 and 2 were 42% and 6%, respectively).

Finally, the inference was repeated using spherical ROIs centered on the mean coordinates of the right cytoarchitectonically defined area 3b ($x = 39.5$, $y = -29$, $z = 55$). No significant activation was detected within a 15 mm sphere around these coordinates. This lack of activation can be explained by the elongated geometry of area 3b and the curvature of the cortex, which is dissimilar to the shape of a sphere. When the small volume correction was repeated with a spherical ROI of 20 mm radius, a significant activation on the postcentral gyrus was found for each subject (Fig. 6, third column in each row). In all subjects, this activation was located slightly lateral and posterior to the significant activation in the MPM-based inference. When the location of these activations following conventional small volume correction was compared to the probabilistic cytoarchitectonic maps of the somatosensory cortex (Fig. 6, forth column in each row), it became evident that these activations were in fact not located in area 3b, but rather in areas 1 and 2.

The present analysis of 3 subjects thus illustrates the following important points:

First, using a whole brain correction often provides very conservative thresholds. That is, correcting for the brain wide family wise error rate may cause false negative results due to its low sensitivity. On the other hand, the application of a small volume correction to control the family wise error rate in a search volume where the activation is *a priori* hypothesized to occur, can considerably increase the sensitivity of the inference and thus reduce false negative results.

Secondly, spherical ROIs are subjectively defined, as the radius of the sphere may be manipulated to yield the desired results. If, on the other hand, the radius of the spherical ROI is not subjectively adjusted, but rather selected based on objective criteria, e.g., by matching its volume to the volume of the hypothesized area, false negative results are likely to occur such as in our example data. No activation was detected in the 15 mm spheres within the hand of area 3b in any of the three subjects.

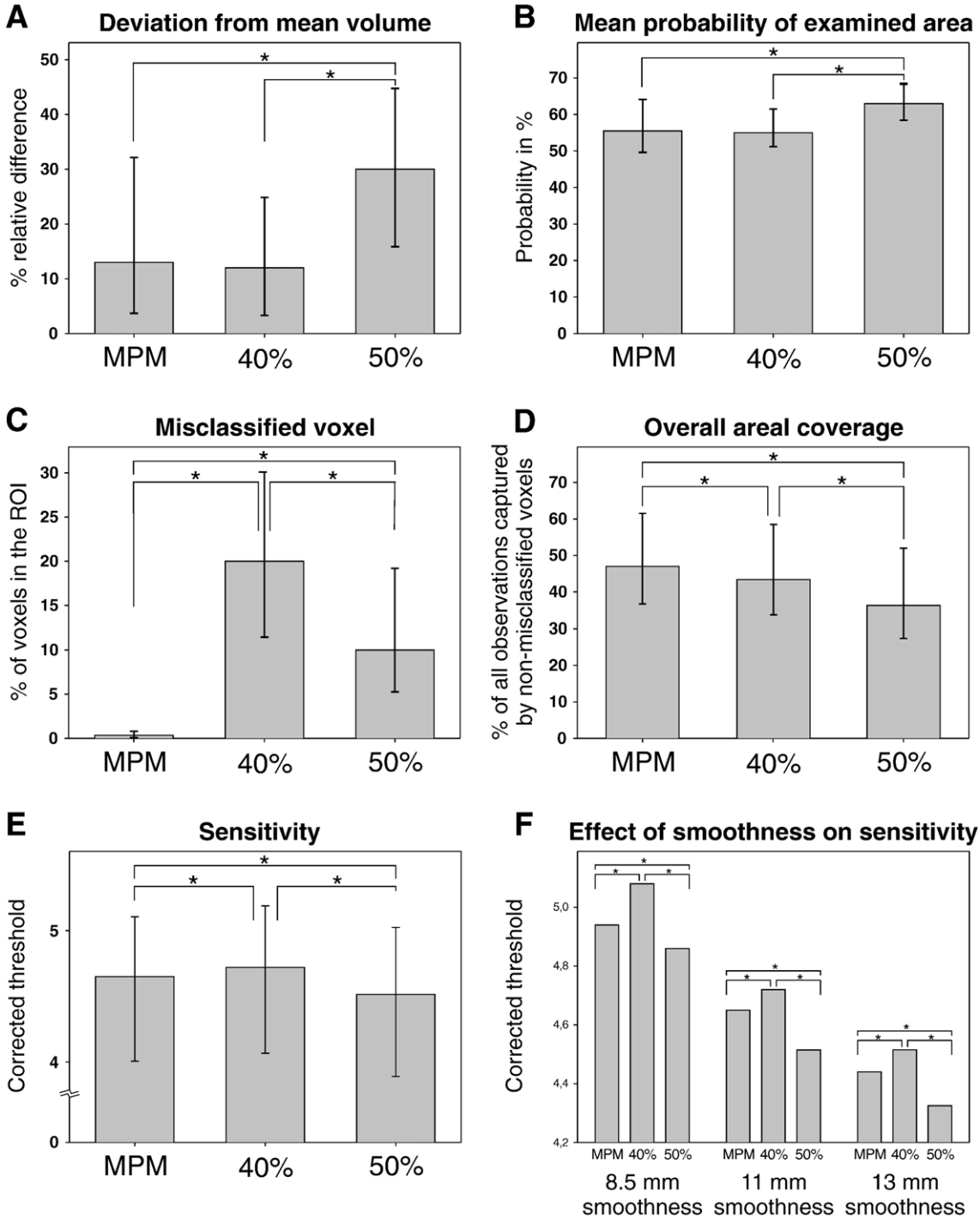

Fig. 5. Mean and standard deviation of the examined measures for anatomical specificity and functional sensitivity across all 36 individual ROIs, defined by the MPM, the 40% maps and the 50% maps. Asterisks mark significant differences ($P < 0.05$, corrected for multiple comparisons). (A) Relative deviation of the ROI's volume from the mean volume of the respective area, expressed in percent. These values are absolute values, not taking into account the direction of the deviation (smaller or larger). (B) Mean probability for the examined area across the voxels included in the ROI definition in percent. (C) Percentage of voxels, which were included in the ROI but had a higher probability of belonging to a different area ("misclassified voxels"). (D) 'Overall areal coverage'. This summary statistic of the anatomical representation is defined by multiplying the number of non-misclassified voxels in the ROI by their mean probability, normalized by the mean size of the respective area, indicating the relative amount of all cytoarchitectonic observations (in any postmortem brain) captured by the ROI (excluding misclassified voxels). (E) Critical threshold for a corrected significance level of $P < 0.05$ in a Gaussian random field (t statistics, 15 degrees of freedom, isotropic smoothness of 11 mm FWHM), indicating the sensitivity for functional activations within the ROIs. Asterisks mark significant differences between the three values measured for the three different methods of defining anatomical ROIs ($P < 0.05$, corrected for multiple comparisons). (F) Replication of the results shown in panel E for different levels of assumed smoothness in the Gaussian random field.

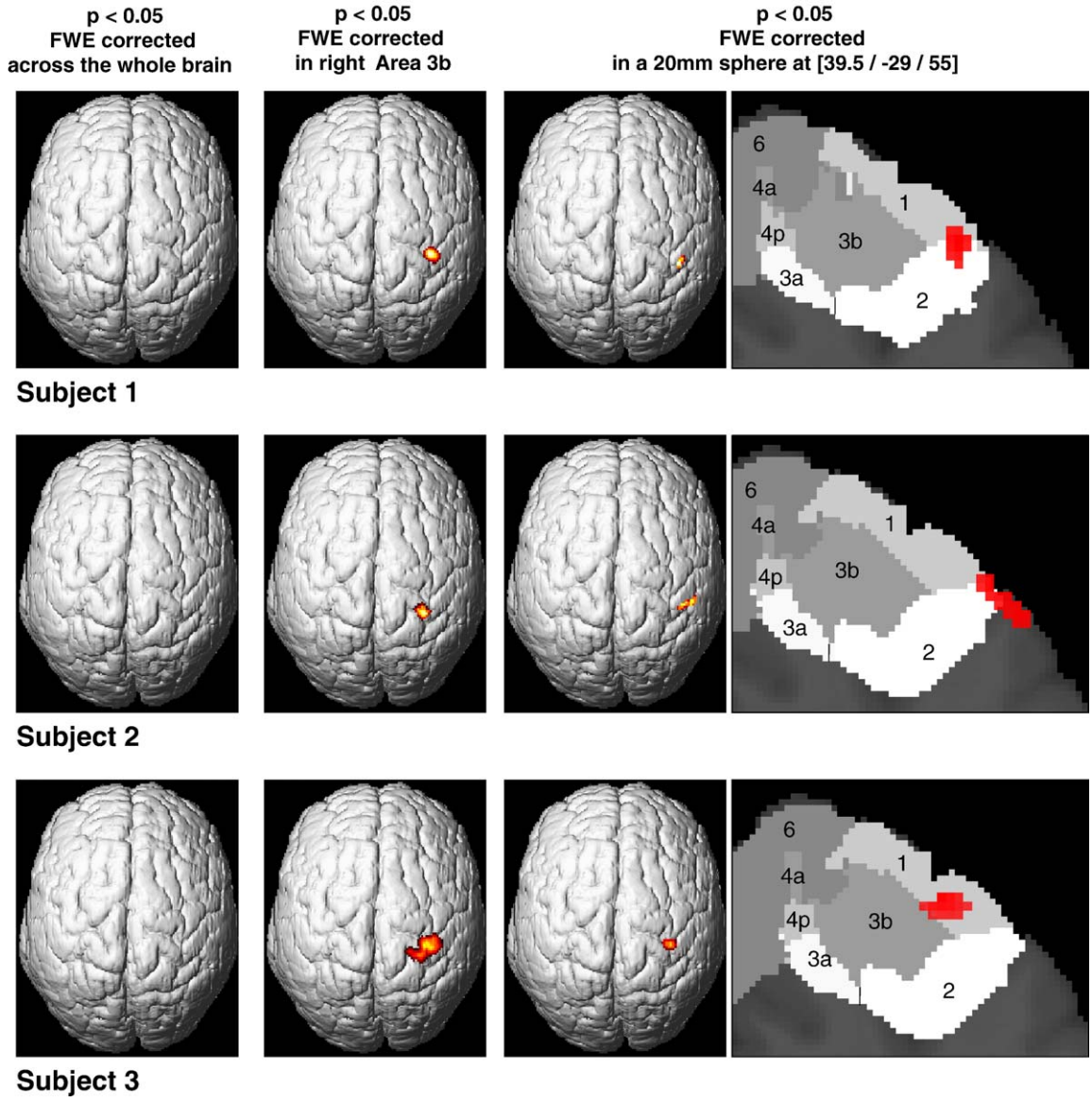

Fig. 6. Results of the exemplary fMRI data sets, showing the significant ($P < 0.05$, corrected for the family wise error rate, FWE) activations following tactile stimulation of the left hand. The first image in each row shows the inference based on whole brain correction. The second image shows the results following the small volume correction for right Area 3b as defined by the MPM. The final two images show the significant activation as defined by a small volume correction in a spherical ROI around the center of gravity for Area 3b, displayed as a surface rendering and in comparison to the MPM of the postcentral gyrus.

Finally, although the hypothesis was formulated explicitly regarding activation in area 3b, the inference based on spherical ROIs, placed around the mean coordinates of that area, revealed activation in two other cytoarchitectonic areas, namely area 1 and area 2. Since activation in these two areas, however, was not hypothesized *a priori*, and can thus strictly speaking not be considered a result of the performed analysis.

Discussion

In this paper, we evaluated different methods for defining ROIs that allow testing anatomical hypothesis in functional neuroimaging based on *a priori* anatomical information. In particular, three methods for defining anatomical ROIs (MPM, 40% maps and 50% maps) and three spherical ROI definitions (5, 10 and 15 mm radius) were compared with respect to their anatomical specificity and functional sensitivity.

The comprehensive analysis of ROIs for three exemplary areas created by the different methods revealed that spherical ROIs represented the least adequate tool for testing anatomical hypothesis in functional neuroimaging. While the mean probabilities for the respective areas within smaller spheres were close to those observed within anatomical ROIs (ROIs based on the MPM or simple thresholding), these spheres comprised only a small proportion of the mean areal volume. This was always true for spheres with a 5 mm radius. However, it was also often true for spheres with a radius of 10 mm, in particular if the hypothesized anatomical area was rather large (Table 2). These spheres thus underestimate the total volume of the respective areas and did not provide a sufficient ‘areal coverage’. Larger spheres on the other hand contained a large proportion of misclassified voxels from

neighboring areas. Furthermore, the mean probabilities for the respective cytoarchitectonic areas within these spheres were much lower than those within anatomical ROIs. These finding was not surprising, since virtually all cortical areas have irregular shapes (cf. Fig. 4), which can hardly be captured by spherical ROIs. Based on our data, cytoarchitectonic probability maps thus provide more valid ROIs for testing of anatomical hypotheses in functional imaging studies and atlassing than the widely used spherical ROIs.

All three methods for the definition of anatomical ROIs (40% and 50% maps, MPM) represented trade-offs between the different measures of anatomical specificity (mean probability, size deviation, fraction of misclassified voxels, 'overall areal coverage'). 50% maps showed the highest mean probabilities but considerably underestimated the size of the respective areas and provided the lowest 'overall areal coverage'. 40% maps in contrast provided a better representation of the cytoarchitectonic volume. However, these ROIs included the largest proportion of misclassified voxels (up to more than 30%). ROIs based on the MPM finally provide a sufficient 'coverage' of the cytoarchitectonic volume. Their mean probabilities are comparable to those of the 40% maps. The main advantage of MPM-based ROIs, however, is the virtual absence of misclassified voxels. The substantial amount of misclassified voxels in the 50% maps might seem illogical, since they would result in a joint probability of more than 100%. However, such voxels are encountered quite frequently, due to the effects of interpolation during spatial normalization, the smoothing applied during the computation of probabilistic maps and most importantly the fact, that different areas were delineated in slightly different sets of subjects.

The sensitivity to functional activations was parameterized by the lowest t value declared significant when correcting for multiple comparisons in the ROI volume (FWE correction at $P < 0.05$). Since all other parameters of the simulated random field were fixed, this critical value depends only on the resel count of the ROI. The resel count $R_d(V)$ in turn is a unitless quantity which depends only on the d-dimensional features (i.e., the size and geometry) of the search region V in resel space (it can be derived by dividing the coordinates of the voxels which define the search volume by the smoothness of the examined data in the corresponding directions) (Worsley et al., 1996). The resel count of a specific ROI can therefore be regarded as a direct measure of its functional sensitivity. In general, the sensitivity of anatomical ROIs was lower than the sensitivity of the spheres. This observation is mainly caused by the considerably larger resel surface area and diameter of the anatomical ROIs relative to their volume. This is in agreement with the notion of Worsley et al. (1996) that spheres represent the "optimal" search volume, covering the largest volume at the lowest overall resel count.

The statistical analysis of ROIs for all available cytoarchitectonic areas, each defined by the three anatomical criteria (MPM, 40% maps, 50%), confirmed the qualitative observations from the three exemplary areas discussed above: the mean probability within the 50% maps was significantly higher than that within ROIs based on 40% maps and the MPM. The deviation of the 40% maps from the mean histological volume, however, was significantly larger than that of either MPMs or 40% maps. MPMs and 40% maps were not significantly different from each other with respect to their mean probability or their volume deviation. The MPMs were superior to both other methods (40% maps, 50% maps) with respect to the amount of misclassified voxels within the ROI as well as with respect to the 'overall areal coverage'. The latter observation is of particular relevance, since this measure describes the faction of all individual cytoarchitectonic observations (in the 10 examined postmortem brains) captured unambiguously by the ROI. It can thus be concluded that the MPM provides the best overall quality of anatomical representation among the three examined methods for defining anatomical ROIs. Furthermore, MPM-based ROIs were also shown to be significantly more sensitive to functional activations than ROIs defined by 40% maps.

MPMs can be considered to provide the most appropriate ROIs for testing anatomical hypotheses in functional neuroimaging. Moreover, defining ROIs by the MPM has the additional advantage that multiple areas can easily be combined. For example, if activation anywhere in "Broca's area" is hypothesized, the MPM representations of areas 44 and 45 can be combined into a single ROI. Due to the nature of the MPM, this ROI will be a continuous volume without any overlap or holes between areas. They are thus closer to the cortical topology as a simple combination of 40% or 50% maps.

Conclusion and implementation

The use of anatomical ROIs has major advantages over the traditional approaches used to define ROIs for small volume corrections. (I) A definition based on probabilistic anatomical maps is completely independent from the functional data analyzed and thus represents a genuine *a priori* hypothesis. (II) In contrast to the traditional ROIs (i.e., spheres, boxes), which require interaction and decisions by the investigator, this algorithmic approach is completely objective. This may improve the comparability of results from different studies. (III) Considering evidence from studies of non-human primates that the microstructure and connectional architecture of the cortex are the main determinants of its functions (Luppino et al., 1991; Matelli et al., 1991), there is a general consensus that cortical areas can be regarded as functional modules of the cortex (Felleman and Van Essen, 1991; Passingham et al., 2002). Therefore, microstructural areas represent the most appropriate reference for regionally specific hypotheses in functional imaging studies.

A software routine of the computation of ROIs based on the cytoarchitectonic MPM as well as a tool for the calculation and visualization of small volume corrections for functional imaging data based on these ROIs has been implemented as part of the SPM Anatomy toolbox (Eickhoff et al., 2005) which is an open source software package freely available for download at www.fz-juelich.de/ime/spm_anatomy_toolbox.

Acknowledgments

This Human Brain Project/Neuroinformatics research was funded by the National Institute of Biomedical Imaging and Bioengeneering, the National Institute of Neurological Disorders and Stroke and the National Institute of Mental Health. K.Z. acknowledges funding by the Deutsche Forschungsgemeinschaft (KFO-112) and the Volkswagenstiftung.

References

Amunts, K., Zilles, K., 2001. Advances in cytoarchitectonic mapping of the human cerebral cortex. Neuroimaging Clin. N. Am. 11, 151–169 (vii).

Amunts, K., Schleicher, A., Burgel, U., Mohlberg, H., Uylings, H.B., Zilles, K., 1999. Broca's region revisited: cytoarchitecture and intersubject variability. J. Comp. Neurol. 412, 319–341.

Amunts, K., Malikovic, A., Mohlberg, H., Schormann, T., Zilles, K., 2000. Brodmann's areas 17 and 18 brought into stereotaxic space—Where and how variable? NeuroImage 11, 66–84.

Amunts, K., Weiss, P.H., Mohlberg, H., Pieperhoff, P., Eickhoff, S., Gurd, J.M., Marshall, J.C., Shah, N.J., Fink, G.R., Zilles, K., 2004. Analysis of verbal fluency in cytoarchitectonically defined stereotaxic space—The roles of Brodmann's areas 44 and 45. NeuroImage 22, 42–56.

Binkofski, F., Amunts, K., Stephan, K.M., Posse, S., Schormann, T., Freund, H.J., Zilles, K., Seitz, R.J., 2000. Broca's region subserves imagery of motion: a combined cytoarchitectonic and fMRI study. Hum Brain Mapp. 11, 273–285.

Bodegard, A., Ledberg, A., Geyer, S., Naito, E., Zilles, K., Roland, P.E., 2000. Object shape differences reflected by somatosensory cortical activation. J. Neurosci. 20, RC51.

Brett, M., Johnsrude, I.S., Owen, A.M., 2002. The problem of functional localization in the human brain. Nat Rev Neurosci 3, 243–249.

Brodmann, K., 1909. Vergleichende Lokalisationslehre der Groβhirnrinde. Barth, Leipzig.

Chau, W., McIntosh, A.R., 2005. The Talairach coordinate of a point in the MNI space: how to interpret it. Neuroimage 25, 408–416.

Collins, D.L., Neelin, P., Peters, T.M., Evans, A.C., 1994. Automatic 3D intersubject registration of MR volumetric data in standardized Talairach space. J. Comput. Assist. Tomogr. 18, 192–205.

Eickhoff, S.B., Stephan, K.E., Mohlberg, H., Grefkes, C., Fink, G.R., Amunts, K., Zilles, K., 2005. A new SPM toolbox for combining probabilistic cytoarchitectonic maps and functional imaging data. NeuroImage 1 (25 (4)), 1325–1335.

Eickhoff, S.B., Zilles, K., Schleicher, A., Amunts, K., 2006a. The human parietal operculum: I. Cytoarchitectonic mapping of subdivisions. Cereb. Cortex 16 (2), 254–267.

Eickhoff, S.B., Amunts, K., Mohlberg, H., Zilles, K., 2006b. The human parietal operculum: II. Stereotaxic maps and correlation with functional imaging results. Cereb. Cortex 16 (2), 268–279.

Eickhoff, S.B., Weiss, P.H., Amunts, K., Fink, G.R., Zilles, K., in press. Identifying human parietal-insular vestibular cortex using fMRI and cytoarchitectonic mapping. Hum. Brain Mapp. (Electronic publication ahead of print)

Evans, A.C., Marrett, S., Neelin, P., Collins, L., Worsley, K., Dai, W., Milot, S., Meyer, E., Bub, D., 1992. Anatomical mapping of functional activation in stereotactic coordinate space. NeuroImage 1, 43–53.

Felleman, D.J., Van Essen, D.C., 1991. Distributed hierarchical processing in the primate cerebral cortex. Cereb. Cortex 1 (1), 1–47 (Jan–Feb).

Geyer, S., 2003. The Microstructural Border Between the Motor and the Cognitive Domain in the Human Cerebral Cortex. Springer, Wien.

Geyer, S., Ledberg, A., Schleicher, A., Kinomura, S., Schormann, T., Burgel, U., Klingberg, T., Larsson, J., Zilles, K., Roland, P.E., 1996. Two different areas within the primary motor cortex of man. Nature 382, 805–807.

Geyer, S., Schleicher, A., Zilles, K., 1999. Areas 3a, 3b, and 1 of human primary somatosensory cortex: 1. Microstructural organization and interindividual variability. NeuroImage 10, 63–83.

Geyer, S., Schormann, T., Mohlberg, H., Zilles, K., 2000. Areas 3a, 3b, and 1 of human primary somatosensory cortex: Part 2. Spatial normalization to standard anatomical space. NeuroImage 11, 684–696.

Grefkes, C., Geyer, S., Schormann, T., Roland, P., Zilles, K., 2001. Human somatosensory area 2: observer-independent cytoarchitectonic mapping, interindividual variability, and population map. NeuroImage 14, 617–631.

Grol, M.J., de Lange, F.P., Verstraten, F.A., Passingham, R.E., Toni, I., 2006. Cerebral changes during performance of overlearned arbitrary visuomotor associations. J. Neurosci. 26, 117–125.

Heim, S., Alter, K., Ischebeck, A.K., Amunts, K., Eickhoff, S.B., Mohlberg, H., Zilles, K., von Cramon, D.Y., Friederici, A.D., 2005. The role of the left Brodmann's areas 44 and 45 in reading words and pseudowords. Cogn. Brain Res. 25, 982–993.

Holmes, C.J., Hoge, R., Collins, L., Woods, R., Toga, A.W., Evans, A.C., 1998. Enhancement of MR images using registration for signal averaging. J. Comput. Assist. Tomogr. 22, 324–333.

Horwitz, B., Amunts, K., Bhattacharyya, R., Patkin, D., Jeffries, K., Zilles, K., Braun, A.R., 2003. Activation of Broca's area during the production of spoken and signed language: a combined cytoarchitectonic mapping and PET analysis. Neuropsychologia 41, 1868–1876.

Hurlemann, R., Matusch, A., Eickhoff, S.B., Palomero-Gallagher, N., Meyer, P., Boy, C., Maier, W., Zilles, K., Amunts, K., Bauer, A., 2005. Analysis of neuroreceptor PET data based on cytoarchitectonic maximum probability maps—A feasibility study. Anat. Embryol. (Berl) 5–6, 453.

Kell, C.A., von Kriegstein, K., Rösler, A., Kleinschmidt, A., Laufs, H., 2005. The sensory cortical representation of the human penis: revisiting somatotopy in the male homunculus. J. Neurosci. 25, 5984–5987.

Kiebel, S., Holmes, A.P., 2003. The general linear model. In: Frackowiak, R.S., Friston, K.J., Frith, C.D., Dolan, R.J., Price, C.J., Ashburner, J., Penny, W.D., Zeki, S. (Eds.), Human Brain Function. Academic Press.

Lancaster, J.L., et al., 2000. Automated Talairach atlas labels for functional brain mapping. Hum. Brain Mapp. 10, 120–131.

Larsson, J., Amunts, K., Gulyas, B., Malikovic, A., Zilles, K., Roland, P.E., 1999. Neuronal correlates of real and illusory contour perception: functional anatomy with PET. Eur J Neurosci. 11, 4024–4036.

Luppino, G., Matelli, M., Camarda, R.M., Gallese, V., Rizzolatti, G., 1991. Multiple representations of body movements in mesial area 6 and the adjacent cingulate cortex: an intracortical microstimulation study in the macaque monkey. J. Comp. Neurol. 311, 463–482.

Maldjian, J.A., Laurienti, P.J., Kraft, R.A., Burdette, J.H., 2003. An automated method for neuroanatomic and cytoarchitectonic atlas-based interrogation of fMRI data sets. NeuroImage 19, 1233–1239.

Matelli, M., Luppino, G., Rizzolatti, G., 1991. Architecture of superior and mesial area 6 and the adjacent cingulate cortex in the macaque monkey. J. Comp. Neurol. 311, 445–462.

Morosan, P., Rademacher, J., Schleicher, A., Amunts, K., Schormann, T., Zilles, K., 2001. Human primary auditory cortex: cytoarchitectonic subdivisions and mapping into a spatial reference system. NeuroImage 13, 684–701.

Naito, E., Ehrsson, H.H., Geyer, S., Zilles, K., Roland, P.E., 1999. Illusory arm movements activate cortical motor areas: a positron emission tomography study. J. Neurosci. 19, 6134–6144.

Naito, E., Roland, P.E., Grefkes, C., Choi, H.J., Eickhoff, S., Geyer, S., Zilles, K., Ehrsson, H.H., 2005. Dominance of the right hemisphere and role of area 2 in human kinesthesia. J. Neurophysiol. 93, 1020–1034.

Noppeney, U., Friston, K.J., Ashburner, J., Frackowiak, R., Price, C.J., 2005. Early visual deprivation induces structural plasticity in gray and white matter. Curr. Biol. 15, R488–R490.

Passingham, R.E., Stephan, K.E., Kotter, R., 2002. The anatomical basis of functional localization in the cortex. Nat. Rev., Neurosci. 3 (8), 606–616 (Aug).

Penny, W.D., Holmes, A.P., 2003. Random effects analysis. In: Frackowiak, R.S., Friston, K.J., Frith, C.D., Dolan, R.J., Price, C.J., Ashburner, J., Penny, W.D., Zeki, S. (Eds.), Human Brain Function. Academic Press, San Diego.

Rademacher, J., Morosan, P., Schormann, T., Schleicher, A., Werner, C., Freund, H.J., Zilles, K., 2001. Probabilistic mapping and volume measurement of human primary auditory cortex. NeuroImage 13, 669–683.

Talairach, J., Tournoux, P., 1988. Co-Planar Stereotaxic Atlas of the Human Brain. Thieme, Stuttgart.

Timm, N.H., 2002. Applied Multivariate Analysis. Springer, New York.
Worsley, K.J., 2003. Developments in random field theory. In: Frackowiak, R.S., Friston, K.J., Frith, C.D., Dolan, J., Price, C.J., J.Ashburner, W.D., Penny, S. (Eds.), Human Brain Function. Academic Press.
Worsley, K.J., Marrett, S., Neelin, P., Vandal, A.C., Friston, K.J., Evans, A.C., 1996. A unified statistical approach for determining significant signals in images of cerebral activation. Hum. Brain Mapp. 4, 58–74.
Young, J.P., Herath, P., Eickhoff, S., Choi, J., Grefkes, C., Zilles, K., Roland, P.E., 2004. Somatotopy and attentional modulation of the human parietal and opercular regions. J. Neurosci. 24, 5391–5399.
Zilles, K., Schleicher, A., Palomero-Gallagher, N., Amunts, K., 2002. Quantitative analysis of cyto- and receptor architecture of the human brain. In: Mazziotta, J., Toga, A. (Eds.), Brain Mapping, the Methods, 2nd ed. Academic Press, San Diego, pp. 573–602.
Zilles, K., Eickhoff, S., Palomero-Gallagher, N., 2003. The human parietal cortex: a novel approach to its architectonic mapping. Adv. Neurol. 93, 1–21.